Taking Advantage of Electrostatic Interactions To Grow Langmuir−Blodgett Films Containing Multilayers of the Phospholipid Dipalmitoylphosphatidylglycerol

Pedro H. B. Aoki,[†] Priscila Alessio,[†,‡,§] M. L. Rodríguez-Méndez,[‡] J. A. De Saja Saez,[§] and Carlos J. L. Constantino*,[†]

[†]*Departamento de Física, Química e Biologia, Faculdade de Ciências e Tecnologia, UNESP, 19060-900 Presidente Prudente, SP, Brazil,* [‡]*Inorganic Chemistry Department, E. T. S. Ingenieros Industriales, University of Valladolid, 47011 Valladolid, Spain, and* [§]*Condensed Matter Physics Department, Faculty of Science, University of Valladolid, 47011 Valladolid, Spain*

The use of phospholipids as mimetic systems for studies involving the cell membrane is a well-known approach. In this context, the Langmuir and Langmuir−Blodgett (LB) methods are among the main techniques used to produce ordered layers of phospholipids structured as mono- or bilayers on water subphase and solid substrates. However, the difficulties of producing multilayer LB films of phospholipids restrict the application of this technique depending on the sensitivity of the experimental analysis to be conducted. Here, an alternative approach is used to produce LB films containing multilayers of the negative phospholipid dipalmitoylphosphatidylglycerol (DPPG). Inspired by the electrostatic layer-by-layer (LbL) technique, DPPG multilayer LB films were produced by transferring the DPPG Langmuir monolayers from the water subphase containing low concentrations of the cationic polyelectrolyte poly(allylamine hydrochloride) (PAH) onto solid substrates. Fourier transform infrared (FTIR) absorption spectroscopy revealed that the interactions between the NH_3^+ (PAH) and PO_4^- (DPPG) groups might be the main driving forces that allow growth of these LB films. Besides, ultraviolet−visible (UV−vis) absorption spectroscopy showed that the multilayer LB films can be grown in a controlled way in terms of thickness at nanometer scale. Cyclic voltammetry showed that DPPG and PAH are more packed in the LB than LbL films. The latter finding is related to the distinct molecular architecture of the films since DPPG is structured as monolayers in the LB films and multilamellar vesicles in the LbL films. Despite the interaction with PAH, cyclic voltammetry also showed that DPPG retains its biological activity in LB films, which is a key factor since this makes DPPG a suitable material in sensing applications. Therefore, multilayer LB films were deposited onto Pt interdigitated electrodes forming sensing units, which were applied in the detection of a phenothiazine compound [methylene blue (MB)] using impedance spectroscopy. The performance of DPPG in single-layer and multilayer LB films was compared to the performance of sensing unities composed of DPPG in single-layer and multilayer LbL films, showing the importance of both the thickness and the molecular architecture of the thin films. As found in a previous work for LbL films, the high sensitivity reached by these sensing units is intimately related to changes in the morphology of the film as evidenced by the micro-Raman technique. Finally, the interaction between MB and the (DPPG + PAH) LB films was complemented by $\pi-A$ isotherms and surface-enhanced resonance Raman scattering (SERRS).

1. Introduction

The lipid fraction of biological membranes is mainly composed of phospholipids with different chain lengths and ionic character.[1] Therefore, phospholipids are widely used as mimetic systems of biological membranes in studies involving the cross resistance to drugs[2] and the development of different compounds such as anesthetics,[3] antibacterial agents,[4] antifungal agents,[5] antibodies against human immunodeficiency virus,[6,7] anti-inflammatory agents,[8] antipsychotic agents,[9] antioxidants,[10] cardiotoxins,[11] biosurfactants,[12] and photosensitizers,[13,14] among others. Usually, these studies are mainly based on the interactions between immobilized biomolecules and drugs or proteins that might be incorporated into artificial membranes, which are mimetic because of the phospholipids structured as mono- or bilayers forming vesicles or Langmuir and Langmuir−Blodgett (LB) films. Consequently, the development or improvement of techniques that allow immobilization of phospholipids onto solid substrates is desirable. In this context, not only the LB method[15−17]

*To whom correspondence should be addressed. E-mail: case@fct.unesp.br.

(1) Lipowski, R.; Sackmann, E. *Handbook of Biological Physics*; Elsevier: Amsterdam, 1995.
(2) Rauch, C. *Eur. Biophys. J.* **2009**, *35*, 537–546.
(3) Nishimoto, M.; Hata, T.; Goto, M.; Tamai, N.; Kaneshina, S.; Matsuki, H.; Ueda, I. *Chem. Phys. Lipids* **2009**, *158*, 71–80.
(4) Zorko, M.; Japelj, B.; Hafner-Bratkovič, I.; Jerala, R. *Biochim. Biophys. Acta* **2009**, *1788*, 314–323.
(5) Miñones, J., Jr.; Pais, S.; Miñones, J.; Conde, O.; Dynarowicz-Łątka, P. *Biophys. Chem.* **2009**, *140*, 69–77.
(6) Matyas, G. R.; Beck, Z.; Karasavvas, N.; Alving, C. R. *Biochim. Biophys. Acta* **2009**, *1788*, 660–665.
(7) Pérez-López, S.; Nieto-Suárez, M.; Mestres, C.; Alsina, M. A.; Haro, I.; Vila-Romeu, N. *Biophys. Chem.* **2009**, *141*, 153–161.
(8) Kundu, S.; Chakraborty, H.; Sarkar, M.; Datta, A. *Colloids Surf., B* **2009**, *70*, 157–161.
(9) Nussio, M. R.; Sykes, M. J.; Miners, J. O.; Shapter, J. G. *Langmuir* **2009**, *25*, 1086–1090.
(10) Suwalsky, M.; Oyarce, K.; Avello, M.; Villena, F.; Sotomayor, C. P. *Chem.-Biol. Interact.* **2009**, *179*, 413–418.
(11) Kao, P. H.; Lin, S. R.; Wu, M. J.; Chang, L. S. *Toxicon* **2009**, *53*, 512–518.
(12) Ortiz, A.; Teruel, J. A.; Espuny, M. J.; Marqués, A.; Manresa, A.; Aranda, F. J. *Chem. Phys. Lipids* **2009**, *158*, 46–53.
(13) Aoki, P. H. B.; Caetano, W.; Volpati, D.; Riul, A., Jr.; Constantino, C. J. L. *J. Nanosci. Nanotechnol.* **2008**, *8*, 4341–4348.
(14) Aoki, P. H. B.; Volpati, D.; Riul, A., Jr.; Caetano, W.; Constantino, C. J. L. *Langmuir* **2009**, *25*, 2331–2338.
(15) Lee, Y. L.; Lin, J. Y.; Chang, C. H. *J. Colloid Interface Sci.* **2006**, *296*, 647–654.
(16) Caseli, L.; Moraes, M. L.; Zucolotto, V.; Ferreira, M.; Nobre, T. M.; Zaniquelli, M. E. D.; Rodrigues-Filho, U. P.; Oliveira, O. N., Jr. *Langmuir* **2006**, *22*, 8501–8508.
(17) Schmidt, T. F.; Pavinatto, F. J.; Caseli, L.; Gonzaga, M. L. C.; Soares, S. A.; Ricardo, N. M. P. S.; Oliveira, O. N., Jr. *J. Colloid Interface Sci.* **2009**, *330*, 84–89.

but also the layer-by-layer (LbL) technique[18−20] or a combination of both LB and LbL techniques[21,22] have been explored in the fabrication of supramolecular architectures with molecular level control.

Dipalmitoylphosphatidylglycerol (DPPG) is a phospholipid extensively applied in studies involving mimetic systems in the form of Langmuir monolayers,[7,13,16,23−25] LB films,[13,16,24−26] unilamellar vesicles,[7,26,27] and multilamellar vesicles.[28,29] Considering preparing a suitable environment either for immobilizing biomolecules or for detecting analytes in solution, we have used both LB[13] and LbL[14] techniques to prepare thin films for both the zwitterionic DPPC and the anionic DPPG. In the latter, the LbL technique was applied as an alternative approach to produce multilayer thin films containing DPPC and DPPG, which are structured as multilamellar vesicles. The possibility of preparing multilayer films opens the perspective of characterizing these mimetic systems using a wider range of techniques in opposition to the LB technique, which usually restricts the phospholipid films to one or two layers.[30] However, despite this disadvantage, the LB technique is still a distinctive way to produce phospholipids structured as mono- or bilayers like they are found in the cell membrane models. Therefore, it is worth pursuing the improvement of methodologies that allow preparation of multilayer films in which the phospholipids are structured as mono- or bilayers.

Here, on the basis of the previous work on multilayer LbL films containing alternating layers of DPPG (multilamellar vesicles) and poly(allylamine hydrochloride) (PAH, cationic polyelectrolyte applied as a "supporting layer"),[14] we have demonstrated the possibility of growing multilayer LB films containing DPPG structured as monolayers. The main information acquired in this study includes (i) the optimized conditions for growing the multilayer LB film of DPPG, (ii) the features of the LB film in terms of thickness control, DPPG−PAH interaction, and molecular packing, and (iii) the performance of the DPPG as a transducer in the LB films when applied in sensing units since it was found that the DPPG sensing properties are highly connected with the maintenance of its biological activity.[13,14] The performance of the DPPG as a transducer in the LB films was compared with the performance of both the multilayer $(PAH/DPPG)_n$ LbL films[14] and the one-layer DPPG LB film[13] previously reported. The growth of the films was monitored by ultraviolet−visible absorption (UV−vis) spectroscopy, while Fourier transform infrared absorption (FTIR) spectroscopy was performed to check the interactions between DPPG and PAH that allow growth of the LB films. Additionally, cyclic voltammetry was applied to compare the molecular packing for both LB and LbL films containing DPPG. Impedance spectroscopy was also conducted for both LB and LbL films containing DPPG deposited onto solid substrates forming sensing units applied in the detection of a phenothiazine compound [methylene blue (MB)] in aqueous solutions. MB was chosen because of its great therapeutic importance in pharmacology as an antimicrobial (bacteria, virus, and fungi) compound and as photosensitizers in photo-antimicrobial chemotherapy,[31] exhibiting physicochemical features associated with both self-aggregation and modification of the properties of natural and model biomembranes upon binding. Besides, it allows us to compare the performance of both LB and LbL films presenting either different thicknesses or distinct molecular architectures with the DPPG being structured in different forms. Finally, the high sensitivity reached by these sensing units was investigated via the micro-Raman technique.

2. Materials and Methods

2.1. Materials. The negative DPPG (1,2-dipalmitoyl-*sn*-glycero-3-[phospho-*rac*-1-glycerol], >99% pure, MW = 745) was purchased from Avanti Polar Lipids Inc. The cationic PAH (MW ∼ 56×10^3) and positive MB (MW = 319) were acquired from Sigma-Aldrich Co. These chemical compounds, the molecular structures of which are shown in Figure 1a, were used as received. The chloroform and methanol (Merck) solvents were HPLC grade. The ultrapure water (18.2 MΩ cm) was acquired from a Milli-Q water purification system (model Simplicity).

2.2. Langmuir and LB Films. The DPPG Langmuir and LB films were fabricated using a Langmuir trough KSV model 2000. The Langmuir films were produced on the water subphase by spreading 100 μL of a 0.74 mg/mL (1.0 mM) DPPG solution dissolved in a methanol/chloroform mixture (1/9 in volume). The Langmuir monolayers were characterized by surface pressure versus mean molecular area ($\pi−A$) isotherms at 23 °C using the Wilhelmy method with the plate surface placed perpendicular to the barriers. The monolayer was symmetrically compressed under a constant barrier speed at 10 mm/min with the subphase containing either ultrapure water or different concentrations of PAH (0.1, 0.01, or 0.001 mg/mL). In addition, DPPG $\pi−A$ isotherms were also recorded for the subphase containing 64×10^{-6} mg/mL MB with and without 0.01 mg/mL PAH.

We obtained the LB films by transferring the DPPG Langmuir monolayers from the air−water interface containing 0.01 mg/mL PAH in the subphase onto different solid substrates depending on the characterization technique to be applied. These films will be termed (DPPG + PAH) LB films. The surface pressure was kept constant at 25 mN/m and the barrier speed at 10 mm/min (symmetrical compression), and upstroke speeds from 0.5 to 3.0 mm/min were used. The deeper speed was varied within this interval during the deposition to keep the transfer ratio (TR) close to 1.0. Under such conditions, Z-type LB films were obtained. LB films containing up to 30 (DPPG + PAH) layers were deposited onto the quartz substrate for UV−vis absorption spectroscopy characterization and 17 (DPPG + PAH) layers onto ZnSe for FTIR measurements. LB films containing one and five (DPPG + PAH) layers were deposited onto Pt interdigitated electrodes (50 pairs of digits with a width of 10 μm, a length of 0.5 mm, and a thickness of 100 nm, 10 μm from each other) for impedance spectroscopy, and 10 (DPPG + PAH) layers were deposited onto ITO electrodes for cyclic voltammetry. In addition, a LB film containing one (DPPG + PAH + MB) layer, with PAH and MB dissolved into the water subphase, was deposited onto a Ag film with a mass thickness of 6 nm produced by thermal evaporation (10^{-7} Torr) for SERRS measurements.

(18) Moraes, M. L.; Batista, M. S.; Itri, R.; Zucolotto, V.; Oliveira, O. N., Jr. *Mater. Sci. Eng., C* **2008**, *28*, 467–471.
(19) Volodkin, D.; Arntz, Y.; Schaaf, P.; Moehwald, H.; Voegel, J. C.; Ball, V. *Soft Matter* **2008**, *4*, 122–130.
(20) Volodkin, D. V.; Schaaf, P.; Mohwald, H.; Voegel, J. C.; Ball, V. *Soft Matter* **2009**, *5*, 1394–1405.
(21) Wang, L. Y.; Schonhoff, M.; Mohwald, H. *J. Phys. Chem. B* **2002**, *106*, 9135–9142.
(22) Ramos, A. P.; Nobre, T. M.; Montoro, L. A.; Zaniquelli, M. E. D. *J. Phys. Chem. B* **2008**, *112*, 14648–14654.
(23) Castillo, J. A.; Pinazo, A.; Carilla, J.; Infante, M. R.; Alsina, M. A.; Haro, I.; Clapes, P. *Langmuir* **2004**, *20*, 3379–3387.
(24) Caseli, L.; Crespilho, F. N.; Nobre, T. M.; Zaniquelli, M. E. D.; Zucolotto, V.; Oliveira, O. N., Jr. *J. Colloid Interface Sci.* **2008**, *319*, 100–108.
(25) Schmidt, T. F.; Caseli, L.; Viitala, T.; Oliveira, O. N., Jr. *Biochim. Biophys. Acta* **2008**, *1778*, 2291–2297.
(26) Morandi, S.; Puggelli, M.; Caminati, G. *Colloids Surf., A* **2008**, *321*, 125–130.
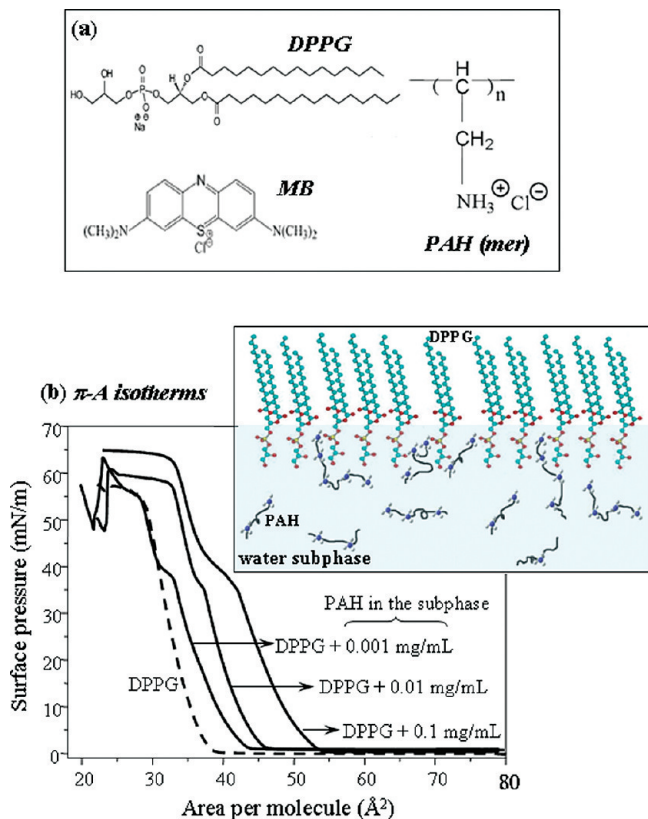(27) Quan, B.; Ianoul, A. *J. Raman Spectrosc.* **2009**, *40*, 260–263.
(28) Chen, J. W.; Shi, K.; Zhang, L.; Huang, F. *Biochem. Biophys. Res. Commun.* **1992**, *186*, 1294–1298.
(29) Castillo, J. A.; Pinazo, A.; Carilla, J.; Infante, M. R.; Alsina, M. A.; Haro, I.; Clapes, P. *Langmuir* **2004**, *20*, 3379–3387.
(30) Girard-Egrot, A. P.; Godoy, S.; Blum, L. J. *Adv. Colloid Interface Sci.* **2005**, *116*, 205–225.

(31) Wainwright, M.; Mohr, H.; Walker, W. H. *J. Photochem. Photobiol., B* **2007**, *86*, 45–58.

Figure 1. (a) Molecular structures of DPPG, PAH (mer), and MB. (b) DPPG $\pi-A$ isotherms recorded for the water subphase containing different concentrations of PAH. The inset is a scheme illustrating the DPPG Langmuir film at the air−water interface with PAH dissolved in the subphase.

2.3. LbL Films. The LbL films were fabricated using DPPG and PAH aqueous solutions at pH 5.6 with concentrations at 0.74 mg/mL (1.0 mM) and 0.80 mg/mL, respectively. All aqueous solutions were prepared without any special procedure: the powder was simply added to ultrapure water and the solution was gently vortexed. The LbL film was fabricated by immersions of the substrate into the distinct solutions according to the following sequence: PAH solution (3 min) → ultrapure water gently stirred to remove excess of adsorbed PAH → DPPG (3 min) → ultrapure water to remove excess of adsorbed DPPG. After that, the first (PAH/DPPG)$_1$ layer is formed and the multilayer (PAH/DPPG)$_n$ LbL film is grown repeating the "four-step sequence". The impedance spectroscopy was carried for (PAH/DPPG)$_1$ and (PAH/DPPG)$_5$ layers deposited onto Pt interdigitated electrodes. The cyclic voltammetry was carried out for (PAH/DPPG)$_{10}$ layers deposited onto ITO electrodes.

2.4. Film Characterization. UV−vis absorption spectroscopy was conducted using a Varian spectrophotometer (model Cary 50) from 190 to 1000 nm, and the FTIR measurements were taken using a Bruker model Tensor 27 spectrometer. Raman analysis and optical microscopy were conducted using a model in-Via micro-Raman Renishaw spectrograph equipped with a Leica microscope, whose 50 × objective lens allows collection of spectra with a spatial resolution of 1 μm^2, a CCD detector, a 633 nm laser, 1800 groove/mm gratings with additional notch filters, and a computer-controlled three-axis-encoded (XYZ) motorized stage to take Raman images with a minimum step of 0.1 μm. The scanning electron microscopy (SEM) image of the SERRS substrate (6 nm Ag film) were recorded using a FEI microscope, model Quanta 200F, and under low vacuum (1.0 Torr).

Cyclic voltammetry was conducted using an EG&G PARC 263A potentiostat/galvanostat (M270 Software) with a conventional three-electrode cell. The reference electrode was an Ag|AgCl/KCl

saturated electrode, and the counter electrode was a platinum plate. The LB and LbL films were immersed in a 5.0 mM haxacyanoferrate(III) aqueous solution (pH 5.6), and the cyclic voltammograms were registered from −0.05 to 0.6 V with the scan rate varying from 5 to 500 mV/s, starting at 0.0 V. In addition, cyclic voltammograms were obtained from −0.7 to 0.0 V with a scan rate at 50 mV/s, starting at 0.05 V, for the LB and LbL films immersed in a 100.0 μM (32.0 μg/mL) or 6.0 μM (1.92 μg/mL) aqueous MB solution (pH 5.6).

The impedance spectroscopy measurements (capacitance and resistance) were taken with a Solartron model 1260A impedance analyzer. The curves were acquired in the frequency range of 1 Hz to 1 MHz, using an amplitude of 50 mV, with the electrodes immersed in ultrapure water, used as reference, and in aqueous MB solutions at 0.01, 1.0, and 100.0 nM. The electrodes were left to soak for 20 min to allow a stable reading, followed by five consecutive runs with each sensing unit to check variations prior to the acquisition of data. Measurements were conducted from the lowest concentration to the highest, and the reference spectra were obtained with ultrapure water. Between each set of measurements, the sensing units were immersed for 10 min in ultrapure water with moderate stirring. It is important to mention that before the sensing units were dipped into a specific MB solution, they were rinsed with the MB solution to avoid interference from the presence of water in the films that might alter the concentration of the measured solution and, consequently, the electrical data.

3. Results and Discussion

3.1. DPPG Langmuir Films ($\pi-A$ isotherms). The DPPG Langmuir films at the air−water interface were prepared with the subphase containing different concentrations of PAH. The corresponding $\pi-A$ isotherms are shown in Figure 1b. Depending on the PAH concentration in the subphase, a shift of the $\pi-A$ isotherms to larger molecular areas is observed. For the subphase pH used here (5.6), the PAH is highly ionized;[32] the same thing happens with DPPG.[33] Therefore, the observed shift of the $\pi-A$ isotherms could be a result of electrostatic interactions between the NH_3^+ and PO_4^- groups of PAH and DPPG, respectively. The molecules of PAH might be placed between the DPPG polar headgroups at the air−water interface (inset of Figure 1b), leading to greater $\pi-A$ isotherm shifting for higher concentrations of PAH. In this case, interactions between the polar headgroups of the DPPG and the nonpolar groups of the PAH chain (hydrophobic interactions) might be weak. Despite the strong ionization of PAH and DPPG at pH 5.6, in a recent work[14] we showed that LbL films containing PAH/DPPG bilayers can be grown without restrictions in terms of the number of bilayers. However, the growth of LbL films containing PAH/DPPC bilayers (dipalmitoylphosphatidylcholine) was restricted to 13 bilayers. The later can be explained by the negative character of DPPG and the zwitterionic character of DPPC, revealing how important the electrostatic interactions are for this system.

Figure 1b also shows that the $\pi-A$ isotherms present an inflection at ca. 38 mN/m, regardless of the PAH concentration in the water subphase. At this surface pressure, PAH molecules might be expelled from the air−water interface into the water subphase. The amount of PAH molecules expelled from the air−water interface depends on the PAH concentration in the subphase. For instance, the condensed phases indicated by the $\pi-A$ isotherms of the DPPG Langmuir films for both the pure water subphase and a PAH concentration of 0.001 mg/mL are coincident. This reveals that all the PAH molecules were expelled from

(32) Shiratori, S. S.; Rubner, M. F. *Macromolecules* **2000**, *33*, 3213−4219.
(33) Boggs, J. M. *Biochim. Biophys. Acta* **1987**, *906*, 353−404.
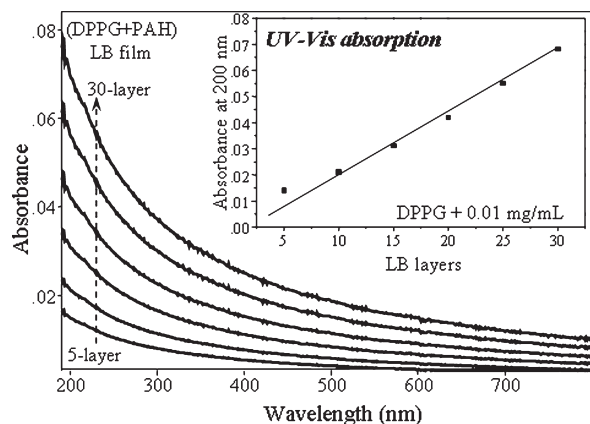
Figure 2. UV−vis absorption spectra of the LB films containing different numbers of layers for the DPPG transferred onto quartz with the water subphase containing 0.01 mg/mL PAH. The inset shows the absorbance at 200 nm vs the number of deposited LB layers.

the air−water interface. On the other hand, for PAH concentrations of 0.01 and 0.1 mg/mL, the $\pi - A$ isotherms indicate that the DPPG Langmuir films form condensed phases with larger areas when compared to the pure water subphase. Therefore, at these concentrations, the PAH molecules are only partially expelled from the air−water interface.

3.2. Growth Mechanism for (DPPG + PAH) LB Films (UV−vis and FTIR). LB films were grown for a constant surface pressure at 25 mN/m. At this value, the DPPG Langmuir films are already well packed onto the water subphase regardless of the PAH concentration as shown by the $\pi - A$ isotherms (Figure 1b). Besides, at this value it is important to ensure that there are PAH molecules at the air−water interface, which was found to be the key factor that allowed the DPPG Langmuir films to be transferred onto solid substrates forming multilayer LB films. The growth of the LB films was monitored using UV−vis absorption spectroscopy. Figure 2 presents the spectra for LB films recorded every five layers up to 30 layers with the water subphase containing 0.01 mg/mL PAH. The inset of Figure 2 shows the absorbance at 200 nm for the different numbers of deposited layers. The absorbance linear growth indicates that the same amount of material is transferred per deposited layer, revealing a controlled growth of the LB films. It is also a strong indication that the substrate itself does not play an important role affecting the structure of the layers, which is an important issue since different substrates must be used depending on the characterization technique applied. The absorbance at 200 nm can be assigned either to DPPG or to PAH.

The presence of both materials in the LB films was confirmed using FTIR in the transmission mode. Figure 3 shows the FTIR spectra for a 17-layer LB film deposited onto ZnSe from the water subphase containing 0.01 mg/mL PAH and cast films of DPPG (from a chloroform solution) and PAH (from an aqueous solution). It is seen that the LB film presents the absorption bands of both DPPG and PAH. However, the DPPG FTIR bands are relatively much more intense than the PAH, indicating that the DPPG is the more abundant material as initially desirable. The DPPG bands at 2917 and 2850 cm^{-1} are assigned to antisymmetric and symmetric CH$_2$ stretchings, respectively; the weak bands at 2954 and 2873 cm^{-1} (observable only under zoom) are attributed to antisymmetric and symmetric CH$_3$ stretchings,

respectively, and the band at 1734 cm^{-1} is assigned to carbonyl group stretching and that at 1465 cm^{-1} to CH$_2$ scissoring.[34,35] Besides, the bands at 1221 and 1094 cm^{-1} for the DPPG cast film are assigned to antisymmetric and symmetric PO$_2^-$ stretchings,[34−36] respectively, and that at 1048 cm^{-1} is assigned to symmetric C−O−C stretching.[36] However, for the (DPPG + PAH) LB film, the band at 1221 cm^{-1} is shifted to 1205 cm^{-1} and the relative intensity of the band at 1094 cm^{-1} is decreased. The latter finding supports the electrostatic interaction between the NH$_3^+$ group of PAH and the PO$_4^-$ group of DPPG (inset of Figure 3) suggested by the $\pi−A$ isotherms of the Langmuir films. Considering the PAH cast film, the band at 3407 cm^{-1} is assigned to N−H stretching, that at 2967 cm^{-1} is assigned to C−H stretching, and those at 1606 and 1511 cm^{-1} are attributed to antisymmetric and symmetric NH$_3^+$ bending vibrations, respectively.[37,38] The bands related to NH$_3^+$ bending vibrations are shifted to 1540 and 1649 cm^{-1} for the (DPPG + PAH) LB films, which is in full agreement with the electrostatic interactions between the NH$_3^+$ and PO$_4^-$ groups. Besides, at higher wavenumbers, the (DPPG + PAH) LB films are completely dominated by the C−H stretching of DPPG and no changes are observed in the FTIR spectra in this region because of the presence of PAH. This supports the suggestion that the phospholipid polar headgroups play a key role in the growth of the LB films containing DPPG and PAH (inset of Figure 3).

3.3. Electrochemical Properties and Molecular Packing of (DPPG + PAH) LB Films. DPPG and PAH can be suitable materials for producing modified electrodes for electrochemical experiments. To investigate the electrochemical behavior of the LB films, cyclic voltammetry experiments were conducted. In addition, an attempt to investigate the possible influence of the different structures and molecular packing presented by DPPG in LB and LbL films (monolayer and multilamellar vesicles, respectively) on the electrochemical and sensing properties was made.

Initially, five cycles between −0.7 and 0.6 V at 50 mV/s were performed for a 10-layer (DPPG + PAH) LB film and a (PAH/DPPG)$_{10}$ LbL film to confirm the absence of any redox process associated with the deposited layers (figure not shown). Then, these ITO-modified electrodes were immersed in a 5.0 mM hexacyanoferrate(III) aqueous solution, and cyclic voltammograms were recorded from −0.05 to 0.6 V at a rate of 50 mV/s. The cyclic voltammograms recorded for LB and LbL are shown in panels a and b of Figure S1, respectively (Supporting Information). In both cases, one anodic wave and one cathodic wave were observed, assigned to[24] Fe^{II}(CN)$_6^{4-}$/Fe^{III}(CN)$_6^{3-}$. Important differences are observed between the electrochemical behaviors of both films. For instance, at 50 mV/s, in the LB films the anodic peak is at 329.6 mV and the cathodic peak was observed at 83.3 mV ($\Delta E = 246.3$ mV). In the LbL films, the separation between the anodic and cathodic peaks was larger ($\Delta E = 398.0$ mV), reflecting a higher degree of irreversibility. Since LB and LbL films have a similar chemical composition, the molecular architecture of the films discussed in previous paragraphs must be in the origin of the distinct voltammograms.

To evaluate the influence of the structure of the films on the kinetics of the redox processes, cyclic voltammograms were registered at 5, 10, 25, 50, 100, 200, 300, 400, and 500 mV/s. Considering the cyclic voltammograms shown in panels a and b of
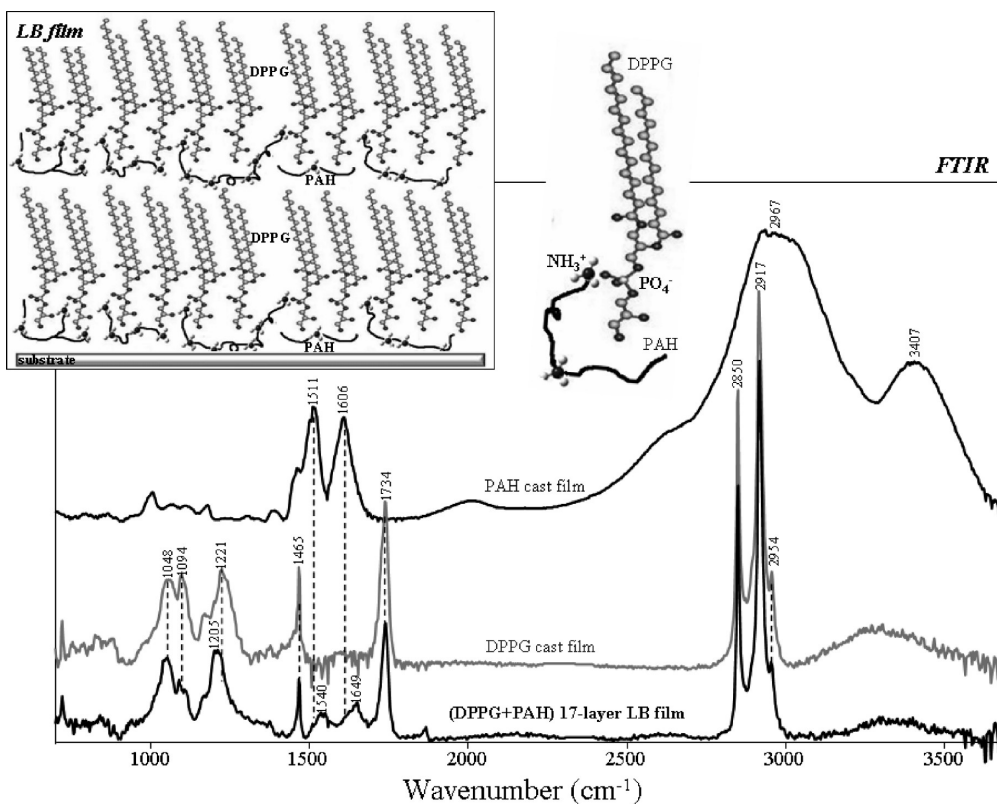
(34) Dicko, A.; Bourque, H.; Pézolet, M. *Chem. Phys. Lipids* **1998**, *96*, 125–139.

(35) Mao, G.; Desai, J.; Flach, C. R.; Mendelsohn, R. *Langmuir* **2008**, *24*, 2025–2034.
(36) Kwon, K. O.; Kim, M. J.; Abe, M.; Ishinomori, T.; Ogino, K. *Langmuir* **1994**, *10*, 1415–1420.
(37) Harris, J. J.; Bruening, M. L. *Langmuir* **2000**, *16*, 2006–2013.
(38) Bonazzola, C.; Calvo, E. J.; Nart, F. C. *Langmuir* **2003**, *19*, 5279–5286.

Figure 3. FTIR spectrum of the 17-layer LB film for the DPPG transferred onto ZnSe with the water subphase containing 0.01 mg/mL PAH. The inset is a scheme illustrating the LB film containing DPPG and PAH. The FTIR spectra of the cast films of PAH and DPPG are given as references.
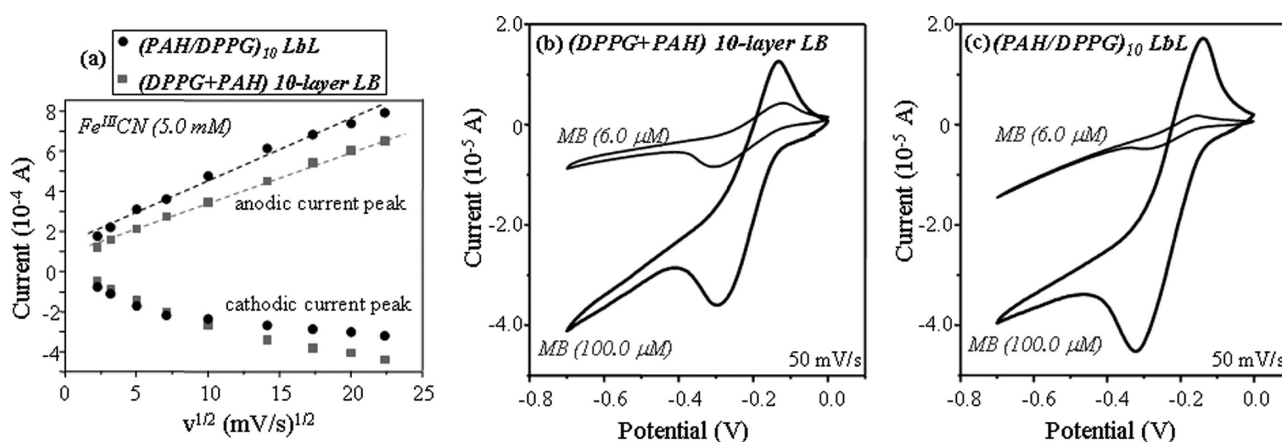
Figure 4. (a) Anodic and cathodic current peaks for the LB and LbL films from cyclic voltammograms recorded with different scan rates in an aqueous hexacyanoferrate(III) solution. Cyclic voltammograms recorded for both (b) LB and (c) LbL films deposited onto ITO and immersed into aqueous MB solutions.

Figure S1 of the Supporting Information, we observed that the electrochemical response is quite distinct for both films. In both cases, the intensity of the peaks increases with scan rate; however, at the same time, the anodic current peaks shift to higher potentials, but the shift is more marked for the LbL films than for the LB films. Figure 4a presents the current intensity (oxidation and reduction peaks) versus scan rate for both films (LB and LbL). It is seen that the anodic current peak (I_a) varies linearly with the square root of the scan rate (v) ($I_a \propto v^{1/2}$), which reveals that the kinetic is controlled by the diffusion of ions. Besides, the curve fitting gives angular coefficients of 0.306 for the LbL film (correlation coefficient $r = 0.989$) and 0.262 ($r = 0.998$) for the LB film, which indicates that the diffusion of the

hexacyanoferrate through the LbL film is easier than in the LB film. The hindering of diffusion of the ion through the LB film suggests that the LB film with the DPPG structured as monolayers is more packed than the LbL film in which the DPPG is structured as multilamellar vesicles. This is a very reasonable assumption since the LB technique imposes a molecular packing when forming the Langmuir film at the air−water interface. A similar effect was found by Caseli et al.[24] working with ITO electrodes modified by a one-layer DPPG LB film with and without enzymes.

Finally, the capabilities of the LB and LbL films to detect MB were also analyzed. The ITO-modified electrodes were immersed into aqueous solutions of MB at 6.0 and 100.0 μM, and cyclic

voltammograms were obtained from −0.7 to 0.0 V at a rate of 50 mV/s [panels b (LB) and c (LbL) of Figure 4]. In this case, a reversible redox pair associated with the oxidation and reduction of MB was observed for both LB and LbL films. We observed that the intensities of the anodic and cathodic peaks are more intense for higher concentrations of MB, being 6.0 μM in the range of the lowest detectable concentrations. In the case of 100.0 μM, the separation between the anodic and cathodic peaks was smaller for LB than for LbL films (ΔE of 162.0 mV for LB films and 185.0 mV for LbL films). However, the differences in reversibility were less marked than in the case of the hexacyanoferrate. This is an important issue because it suggests that the role of the structure of the modifier layer depends on the nature of the detected species.

3.4. Sensing Units (impedance spectroscopy) of (DPPG + PAH) LB Films. The performance of the (DPPG + PAH) LB films as transducers in sensing units was checked by immersing them in aqueous solutions containing MB at different concentrations. This approach was chosen to allow a comparison with previous results obtained using a one-layer LB film of neat DPPG and (PAH/DPPG)$_5$ LbL film.[13,14] Here, the (DPPG + PAH) LB films with one and five layers were deposited onto Pt interdigitated electrodes forming the sensing units. Complementary, Pt interdigitated electrodes were covered with one-layer LB of neat DPPG, and other two Pt electrodes were covered with (PAH/DPPG)$_1$ and (PAH/DPPG)$_5$ LbL films. These five sensing units allow comparison of the effect of both thickness and molecular architecture of the films on the impedance response. The electrical measurements were conducted taking into account some experimental details considering the high sensitivity of the electrodes used. (i) The bare Pt electrodes were carefully tested prior to film deposition in ultrapure water to guarantee similar electrical responses. All of them presented practically indistinguishable electrical responses. (ii) A sequence of measurements every 5 min was conducted with the sensing units dipped in ultrapure water to check the temporal stabilization of the electrical signal due to the formation of a double layer at the electrode−electrolyte interface.[39] The electrical signals start to superpose each other 15 min after the immersion of the electrodes in ultrapure water. Therefore, the sensing units were left to soak for 20 min in the MB solutions before data acquisition to better ensure a stable reading of the data. (iii) In addition, after each set of measurements, the sensing units were carefully washed with ultrapure water to remove possible MB molecules trapped within the films. Five independent measurements made from the same stock solutions were taken for each liquid sample, apart from measurements in ultrapure water before and after the sensing units had been dipped into MB solutions, to better check for possible contamination of the sensing units.

In the Supporting Information, the capacitance versus frequency recorded for ultrapure water before and after all the measurements and for MB aqueous solutions at 0.01, 1.0, and 100 nM using the bare Pt electrode and the five sensing units described previously is presented (Figure S2). Some features can be extracted from the impedance data. (i) It is seen from the water measurements, before and after the sensing units had been exposed to MB, that the capacitance curves are quite close, discarding a MB contamination and suggesting the reusability of the sensor. The latter fact also indicates a weak chemical interaction between the MB and the sensing unit materials. (ii) In contrast to the bare Pt electrode (Figure S2a), considerable

differences appear in the impedance results with the sensing units in ultrapure water and in MB aqueous solutions (Figure S2b−f), revealing that the films affect the electrical response of Pt, in spite of being ultrathin films. (iii) Differences are also seen among the sensing units, even in pure water or at very low concentrations of MB, which points to the high sensitivity of the array as a whole. These differences from one sensing unit to another can be discussed considering both the film thickness (one and five layers) and the methods applied to produce the films (LB and LbL). (iv) With respect to thickness, considering the one-layer LB films (Figure S2b,c), one can see that the presence of PAH improves the ability of the sensing unit to distinguish between the water with and without MB. Being complementary, the thickness effect is observed by comparing the (DPPG + PAH) one- and five-layer LB films (Figure S2c,d). It is clearly seen that the LB film containing five layers is more distinguished than the MB at different concentrations. The thickness effect is seen for the LbL films as well when both (PAH/DPPG)$_1$ and (PAH/DPPG)$_5$ films are compared in panels e and f of Figure S2, respectively. (v) On the other hand, comparing the LB and LbL films (panels c and e of Figure S2 and panels d and f of Figure S2), we observe that the profile of the capacitance curves is the main parameter affected. Once again, the molecular architecture of the thin films in the sensing units might be responsible for these changes in the profile of the spectra, especially because the electrical response is governed by distinct phenomena over different frequency ranges. For instance, in the range from 50 to 200 Hz the response is basically governed by the double layer formed at the interface between the film and the liquid, from 10^2 to 10^5 Hz the response depends strongly on the film properties, while for frequencies higher than 10^5 Hz it is basically determined by the electrode geometry.[39] (vi) In the case of LB films on Pt electrodes, one of the main pieces of information is that the DPPG keeps its biological activity with respect to MB despite the interaction with PAH when forming the multilayer LB film. Similar information was also found for LbL films containing (PAH/DPPG)$_n$.[14] This suggests that only a few DPPG molecules might be necessary to interact with PAH to form the LB multilayer films. The ratio of 2.15 molecules of PAH in the water subphase (volume) for 1.0 molecule of DPPG at the air−water interface supports that.

The high sensitivity expected from the distinct impedance spectra in Figure S2 was confirmed when the experimental data were correlated through principal component analysis (PCA), which is a mathematical method ordinarily employed to find patterns in data, highlighting their similarities and differences.[40] It accounts for the variability of the data, attempting to identify new meaningful variables and reducing the dimensionality of the data set, with a minimum loss of information, forming groups of samples with a high degree of similarity. The original variables are linearly combined by using only variance−mean relationship information, projecting the data in a reduced hyperspace plot defined by the principal components. PC1 has the highest variance of the data set; PC2 has the second largest amount of information (variance), and so on. All the data with regard to the PCA plots is given in the Supporting Information. Figure S3a shows the data taken for a fixed frequency at 10 kHz, which is in a region where a significant variation of the data occurs, for ultrapure water (before and after MB measurements) and MB solutions at 0.01, 1.0, and 100.0 nM. A good distinction of MB solutions from water was achieved, and a good correlation between PC1 and the MB content was also found. Figure S3a

(39) Taylor, D. M.; Macdonald, A. G. *J. Phys. D: Appl. Phys.* **1987**, *20*, 1277–1283.

(40) Gorban, A.; Kegl, B.; Wunsch, D.; Zinovyev, A. *Principal Manifolds for Data Visualisation and Dimension Reduction*; Springer: Berlin, 2007.
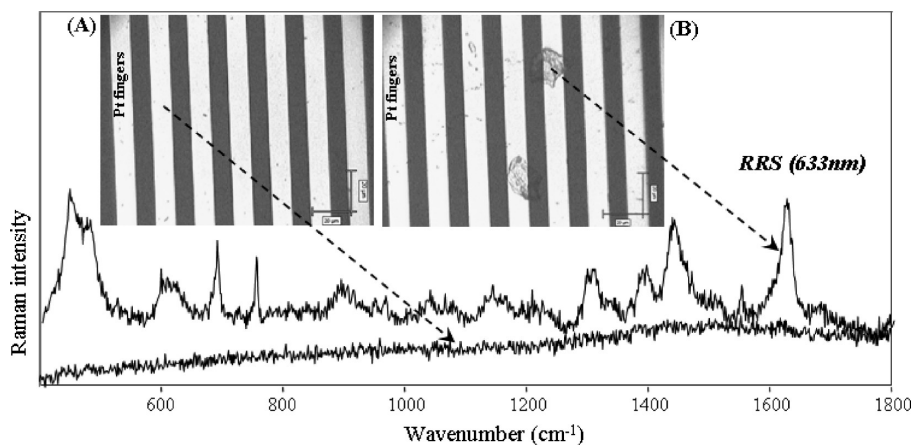
Figure 5. Resonance Raman scattering (RRS) spectra recorded with the 633 nm laser line for the five-layer (DPPG + PAH) LB film deposited onto the Pt interdigitated electrode before (A) and after (B) immersion in the MB solutions. Insets A and B are optical images recorded for this sensing unit before and after immersion in MB solutions. The RRS spectrum from inset B is assigned to MB.

shows that the more concentrated MB clusters are shifted to the left while the water samples are displayed close to each other and on the opposite side on the PC1 axis. A similar trend is found for PC2 with the more concentrated MB solutions shifted to the bottom.

To assess the importance of each sensing unit for the overall high sensitivity, PCA plots were obtained by eliminating one of the sensing units. Panels b−d of Figure S3 present the results of eliminating the LB films and panels e and f of Figure S3 results of removing the LbL films. The plots were slightly affected when the excluded sensing unit was the Pt bare electrode (figure not shown) or the Pt electrode coated with a one-layer DPPG LB film (Figure S3b), a one-layer (DPPG + PAH) LB film (Figure S3c), or a (PAH/DPPG)$_1$ LbL film (Figure S3e). However, the PCA plots were significantly affected by removal of the five-layer (DPPG + PAH) LB film (Figure S3d) followed by the (PAH/DPPG)$_5$ LbL film (Figure S3f). Therefore, it is possible to establish that this trend is intimately connected to the film thickness as already discussed for impedance data. Besides, when these two films are compared, the fact that the absence of the five-layer (DPPG + PAH) LB film leads to a more significant change in the PCA plots reinforces the important role played by the molecular architecture of the films.

The high sensitivity reached by the sensing units formed by interdigitated electrodes covered by LB or LbL films is well-known;[41] however, its origin is still intriguing. Here, taking advantage of the large cross section of the MB with respect to the Raman scattering,[42] we have investigated by a micro-Raman technique the sensing units before and after their immersion in the MB solutions used in the impedance measurements. The micro-Raman technique combines morphological and chemical information by coupling an optical microscope to a Raman spectrograph, which allows spectra from spots with micrometer spatial resolution to be collected.[43] Figure 5 shows the resonance Raman scattering (RRS) spectra obtained with the 633 nm laser line for the five-layer (DPPG + PAH) LB film on the Pt interdigitated electrode before and after immersion in the MB solutions. Insets A and B of Figure 5 show the optical images recorded for this sensing unit before and after its immersion in MB solutions, respectively. It can be seen that RRS spectra can be collected only from aggregates placed on the sensing unit surface and these

aggregates are assigned to the MB.[42] Therefore, we can conclude that in this case, the changes in the morphology of the LB film induced by the presence of MB are responsible for the high sensitivity reached by the sensing unit. Similar results were found in the previous work[14] for LbL films containing the DPPG structured as multilamellar vesicles. Reinforcing that, immersing the LB films in aqueous solutions containing MB even at concentrations higher than those used for impedance spectroscopy, we did not observe any difference either in the FTIR or in the UV−vis absorption spectra. The latter finding is in full agreement with the weak chemical interaction between the MB and the sensing unit materials suggested by impedance data (reusability of the sensing units). A weak chemical interaction between MB and DPPG or DPPC was previously reported[13] for mixed Langmuir films formed by cospreading the MB and the phospholipids at the air−water interface, despite the fact that other phenothiazine compounds such as chlorpromazine and trifluoperazine induce significant changes in the DPPG $\pi−A$ isotherms with drug concentrations of ≤1 mol %.[44]

3.5. Complementary Study of DPPG, PAH, and MB. The weak chemical interaction between MB and DPPG specifically has been revealed using different approaches such as Langmuir films produced by cospreading,[13] one-layer LB films,[13] LbL films,[14] and the multilayer LB films in this work. A complementary study was conducted in an attempt to confirm that the weak interaction between DPPG and MB is not due to the interaction between DPPG and PAH when they form the multilayer LB films. An approach distinct from those described in the previous sections for voltammetry, impedance, FTIR, and UV−vis (immersing the films into an aqueous MB solution and collecting the data before and after that) and reported in refs 13 and 14 was applied. Here, Langmuir films were fabricated by dissolving both PAH and MB in the water subphase. Then, the Langmuir films were transferred onto solid substrates forming a one-layer mixed LB film. This mixed LB film was deposited onto a glass substrate previously covered with a 6 nm Ag film (vacuum thermal evaporation method) to allow collection of the surface-enhanced resonance Raman scattering (SERRS) spectra.
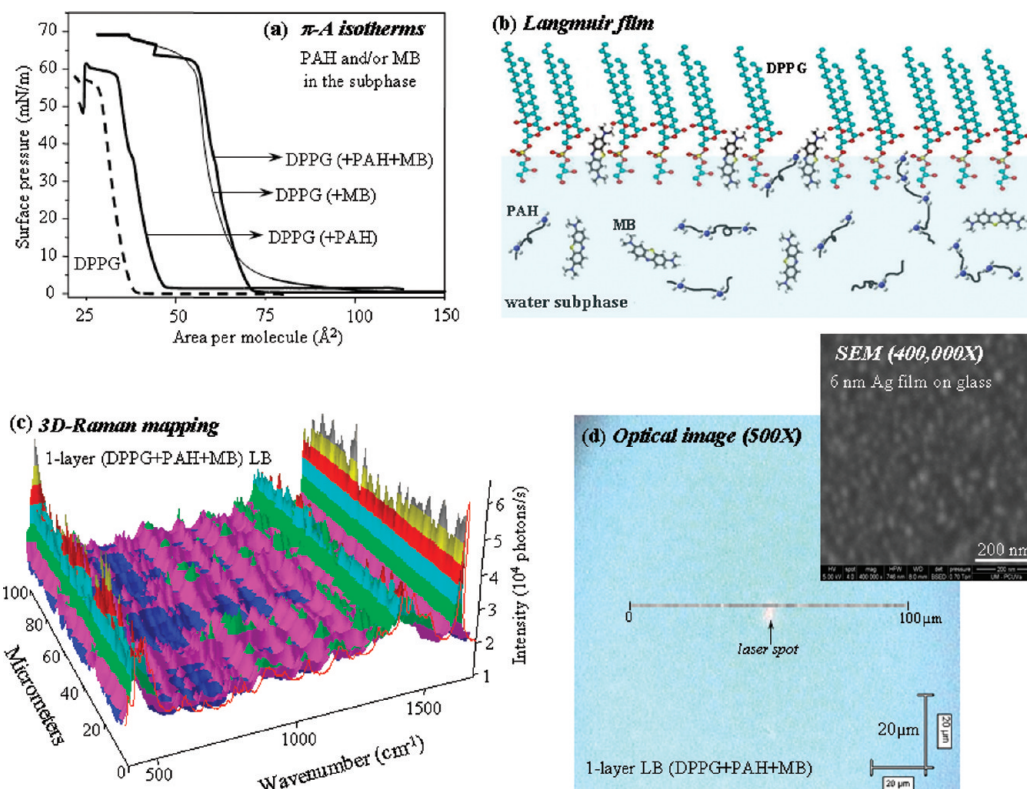
Figure 6a shows the $\pi−A$ isotherms recorded for DPPG at the air−water interface (100 μL spread; 0.74 mg/mL) with the subphase containing PAH (0.01 mg/mL) and MB (64×10^{-6} mg/mL). Under these experimental conditions, there is 1.0 molecule

(41) Riul, A., Jr.; dos Santos, D. S.; Wohnrath, K.; Di Tommazo, R.; Carvalho, A. C. P. L. F.; Fonseca, F. J.; Oliveira, O. N., Jr.; Taylor, D. M.; Mattoso, L. H. C. *Langmuir* **2002**, *18*, 239–245.
(42) Nicolai, S. H. A.; Rubim, J. C. *Langmuir* **2003**, *19*, 4291–4294.
(43) Aroca, R. F.; Constantino, C. J. L. *Langmuir* **2000**, *16*, 5425–5429.
(44) Hidalgo, A. A.; Caetano, W.; Tabak, M.; Oliveira, O. N., Jr. *Biophys. Chem.* **2004**, *109*, 85–104.

Figure 6. (a) DPPG $\pi-A$ isotherms recorded for the water subphase containing either PAH (0.01 mg/mL) or MB (64×10^{-6} mg/mL). (b) Scheme illustrating the DPPG Langmuir film at the air−water interface with PAH and MB dissolved in the subphase. (c) SERRS spectra recorded for the one-layer LB film for the DPPG transferred onto a 6 nm Ag film with the water subphase containing 0.01 mg/mL PAH and 64×10^{-6} mg/mL MB. (d) Optical image of this one-layer LB film on a 6 nm Ag film with the line from where the SERRS spectra were collected point by point. The inset is an SEM image showing the Ag nanoparticles formed by evaporation of 6 nm Ag onto a glass substrate. In all cases, the SERRS spectra are assigned to MB.

of DPPG at the air−water interface for ~2.4 molecules of MB in the water subphase volume and ca. 2.15 molecules of PAH (ca. 2.7×10^3-mers of PAH, mainly formed by NH_3^+ groups since most of PAH molecules are ionized at pH 5.6[32]). The shift of the DPPG $\pi - A$ isotherms for larger areas due to the presence of PAH was discussed in Figure 1b (they are repeated here for better comparison). We observe that the presence of MB, even at concentrations much lower than those of PAH-mers, induces a greater displacement of the DPPG $\pi - A$ isotherms to larger areas. This clearly indicates a higher affinity between DPPG and MB than DPPG and PAH, whcih is desirable considering the DPPG in sensing applications. Figure 6b presents a scheme to illustrate the DPPG Langmuir film formed at the air−water interface in the presence of both PAH and MB in the water subphase.

Finally, Figure 6c presents the SERRS spectra from the one-layer (DPPG + MB + PAH) LB film. The SERRS spectra were collected point by point (1 μm step) along a line of 100 μm leading to 101 spectra, which are displayed in three dimensions forming the three-dimensional Raman image. The SERRS spectra are assigned to the MB,[42] which reveals that the interaction between MB and DPPG is sufficient to transfer the MB from the water subphase to the solid substrate, despite the interaction between DPPG and PAH. The intensity differences in the SERRS spectra in Figure 6c allow us to conclude that the MB is fairly homogeneously distributed on the substrate surface, which is supported by the optical image of the one-layer LB film shown in Figure 6d. The inset in Figure 6d presents an SEM image of the Ag nanoparticles formed on the glass substrate when the Ag is thermally evaporated under vacuum (6 nm mass thickness) to produce the SERRS substrate. The optical image (Figure 6d) also

shows the laser focused in a characteristic spot that is a few micrometers in diameter and the line from where the MB SERRS spectra were collected [the brighter spots indicate more intense signals for the 1622 cm^{-1} Raman band that is assigned to MB (C=C + C−N=C) stretchings[45]].

4. Conclusions

We successfully fabricated Langmuir−Blodgett (LB) films containing multiple layers of the anionic phospholipid DPPG by taking advantage of the electrostatic interaction between the PO_4^- (DPPG) and NH_3^+ (PAH, cationic polyelectrolyte) groups. The interaction was initially suggested by the $\pi - A$ isotherms of the DPPG Langmuir films formed at the air−water interface with the water subphase containing different concentrations of PAH. The DPPG $\pi - A$ isotherms were shifted to larger molecular areas for higher concentrations of PAH in water. The growth of the LB films containing (DPPG+PAH) multilayers was monitored by UV−vis absorption spectra, and the FTIR spectra showed that the amount of DPPG present in the LB film is much higher than the amount of PAH, which is desirable. A comparison between the (DPPG+PAH) LB films and the (PAH/DPPG)$_n$ LbL films was established through cyclic voltammetry and impedance spectroscopy in the presence of the cationic drug methylene blue (MB) in an aqueous solution. The cyclic voltammograms for ITO-modified electrodes by both films in the presence of MB were distinct from that for bare ITO, suggesting that DPPG is biologically active despite the interactions with PAH when forming

(45) Nicolai, S. H. A.; Rodrigues, P. R. P.; Agostinho, S. M. L.; Rubim, J. C. *J. Electroanal. Chem.* **2002**, *527*, 103–111.

the films. The later was confirmed by impedance spectroscopy. Besides, in the presence of an aqueous haxacyanoferrate(III) solution and when the cyclic voltammograms were recorded with the scan rate varying from 5 to 500 mV/s, it was found that the LB films are more packed than the LbL films. This behavior might be mainly related to the distinct molecular architecture assumed by the DPPG molecules in both films (monolayers for LB and multilamellar vesicles for LbL). In terms of impedance spectroscopy, we also found that the molecular architecture of the films deposited onto Pt interdigitated electrodes forming sensing units plays an important role. Besides, the effect of the film thickness on the sensitivity of an array formed by sensing units containing LB and LbL films with a distinct number of layers was exploited for highly diluted aqueous MB solutions (nanomolar level). We found that the thicker LB films followed by the thicker LbL films in the investigated range present a more significant performance for the array sensitivity. Finally, we observed that the MB−DPPG

interaction in the LB or LbL films when these films are immersed in an aqueous MB solution is weak. However, the latter fact should not be assigned to a competition with DPPG−PAH interactions. The $\pi - A$ isotherms revealed a stronger affinity between DPPG and MB than between DPPG and PAH, which was enough to transfer the MB trapped in the DPPG layers when forming LB films as shown by surface-enhanced resonance Raman scattering (SERRS).

Supporting Information Available: Cyclic voltammetry, impedance spectroscopy, and principal component analysis (PCA) data. This material is available free of charge via the Internet at http://pubs.acs.org.